COMMUNICATIONS IN NUMERICAL METHODS IN ENGINEERING
Commun. Numer. Meth. Engng 2008; **24**:297–320
Published online 5 March 2007 in Wiley InterScience (www.interscience.wiley.com). DOI: 10.1002/cnm.969

Study of a stabilized mixed finite element with emphasis on its numerical performance for strain localization problems

P. J. Sánchez[1,2,*,†], V. E. Sonzogni[1] and A. E. Huespe[1]

[1]*Centro Internacional de Métodos Computacionales en Ingeniería* (*CIMEC*), *INTEC-UNL-CONICET*, *Güemes 3450*, *Santa Fe 3000*, *Argentina*
[2]*GIMNI-UTN FRSF*, *Lavaisse 610*, *Santa Fe 3000*, *Argentina*

SUMMARY

The numerical performance of a stabilized mixed finite-element formulation based on the pressure-gradient-projection method (PGP) using equal-order (linear) interpolation is evaluated by solving solid mechanics problems, such as structural limit load determination and strain localization modelling. All of them present incompressibility kinematical constraints induced by the constitutive behaviour. This work is specially devised to obtain critical conclusions about the use of PGP model when the mechanical response is governed by strain-softening macroscopic mechanisms. In this context, we report some detected limitations in the present formulation due to the existence of pathological mesh bias dependence once the strain localization process becomes dominant, and linear kinematics is used. An additional contribution is the numerical comparative analysis of two different strategies, for solving the complete linear equation system, addressed to a finite-element parallel code. The numerical results are compared with the standard Galerkin formulation and with an alternative stabilized mixed finite-element procedure (pressure stabilizing Petrov–Galerkin scheme). Copyright © 2007 John Wiley & Sons, Ltd.

Received 16 June 2006; Revised 24 October 2006; Accepted 30 October 2006

KEY WORDS: mixed finite elements; stabilized formulation; strain softening; localization of plastic deformation; ductile failure

*Correspondence to: P. J. Sánchez, Centro Internacional de Métodos Computacionales en Ingeniería (CIMEC), INTEC-UNL-CONICET, Güemes 3450, Santa Fe 3000, Argentina.
†E-mail: psanchez@intec.unl.edu.ar

Contract/grant sponsor: Consejo Nacional de Investigaciones Científicas y Técnicas (CONICET); contract/grant number: CONICET PIP 5271
Contract/grant sponsor: Agencia Nacional de Promoción de Actividades Científicas y Tecnológicas (ANPCyT); contract/grant number: ANPCyT PICT 14573
Contract/grant sponsor: Universidad Nacional del Litoral (UNL) and Universidad Tecnológica Nacional; contract/grant number: UNL CAI+D 2005-10-65

1. INTRODUCTION

Simplicial low-order standard displacement-based finite elements present several advantages to solve practical problems in the context of solid mechanics such as: robustness, easiness for automatic mesh generation, reduced number of degrees of freedom and minimal final equation system band width, among others. These features mean better efficiency from a computational viewpoint. However, it is well known that the numerical response of the standard Galerkin finite elements, for problems involving isochoric deformations, differs considerably from analytical or experimental results.

Many different strategies have been developed in the standard models to overcome these limitations. The stabilized mixed finite element methods have shown to be robust approaches to reach this objective. Initially, they were used in the computational fluid dynamics (CFD) area. The stabilized strategies consist basically of adding mesh-dependent terms to the usual mixed Galerkin method, which are functions of the residual of the Euler–Lagrange equations. These elementwise evaluated terms insure consistency and incorporate stability. Similar concepts, for compressible and incompressible elasticity and plasticity, have been applied to solid mechanics (see, for example, Wall *et al.* [1], Klaas *et al.* [2]).

This study aims at the numerical evaluation of a stabilized mixed finite element procedure recently introduced [3–7] for incompressible elasticity, perfect von Mises plasticity and, specially, for localization phenomena induced by material instability. The present formulation of the stabilization scheme is similar to that described in these works, and has been implemented by using a linear triangle (or tetrahedral) finite element in displacement with linear ($\mathscr{C}^0$) pressure interpolation.

The main objective of this work is to address some particular aspects of its numerical performance that complement the conclusions exposed in the above cited references, and more importantly, furnishes additional details about its behaviour in challenging problems of solid mechanics. They are: (i) comparison of results with respect to other stabilized mixed alternative method; (ii) parametric study of the stabilization factor that becomes a fundamental ingredient in this model; (iii) stress and displacement convergence rate analysis; and (iv) mesh bias dependence of the results, particularly when plasticity with softening is modelled.

The last point becomes a key aspect of finite element modelling if plastic localization analysis is addressed. In this context, the fact that the linear kinematics of the constant strain triangle (CST) is not well adapted for capturing the strain localization mechanism, is widely recognized. Thus, several publications mention the dependence of the solution with the FE mesh bias. Clearly, this deficient response is not only caused by the isochoric deformation kinematical constraint, because it also is observed when damage models are used. Possible solutions to this drawback have been obtained by introducing an enhanced kinematics, for example, embedding a strong discontinuity mode into the FE [8–11] that can be understood as the inclusion of a new sub-scale in the displacement field approach. In the present pressure-gradient-projection (PGP) formulation, the stabilization strategy can also be understood as the addition of a sub-scale in the displacement field [12]. So, in the paper, we determine if this enrichment is enough for capturing the shear band mode in an objective way.

As an additional contribution, the present formulation has been implemented in the 'PETSc-FEM' general parallel finite element code [13]. Two different solution strategies, to solve the linear equation system, and a novel preconditioner scheme [14], are compared.

The paper is organized as follows: the next section is devoted to an overview of the continuum and discrete forms of the stabilized mixed formulations. In Section 3, those aspects related to

DOI: 10.1002/cnm

the numerical implementation are exposed, with special mention in parallel programming topics. Section 4 presents the numerical 2D and 3D solid mechanics tests, particularly using J2 plasticity. Finally, the conclusions are summarized.

2. STABILIZED MIXED FORMULATION IN SOLIDS MECHANICS

Let us consider a solid mechanics problem with the small deformation assumption. We introduce some notation to define it: Ω is an open bounded set included in $\mathbb{R}^n$ (n is the space dimension) whose points represent those of a continuum body $\mathbb{B}$ in the reference configuration, Γ is the boundary of Ω which can be split in two sub-sets $\Gamma_{\mathbf{u}}$ and $\Gamma_{\boldsymbol{\sigma}}$ where prescribed displacements $\overline{\mathbf{u}}$ and traction $\mathbf{t}$ are imposed.

The uncoupling of the stress tensor $\boldsymbol{\sigma}$ into its spherical ($\sigma_{\mathrm{m}} = \frac{1}{3}\operatorname{tr}(\boldsymbol{\sigma})$) and deviatoric part ($\mathbf{S} = \operatorname{dev}(\boldsymbol{\sigma})$) allows us to write the Cauchy equation, neglecting the inertial forces, as follows:

$$\nabla\sigma_{\mathrm{m}} + \nabla\cdot\mathbf{S} + \rho\mathbf{b} = \mathbf{0} \quad \forall\mathbf{x}\in\Omega \tag{1}$$

$\mathbf{b}$ being the distributed mass forces and ρ the material density.

Introducing the constitutive model equations, the dependence of stresses with the (gradient of) displacements $\mathbf{u}$ can be expressed as:

$$\boldsymbol{\sigma} = \hat{\boldsymbol{\sigma}}(\mathbf{u}) = \hat{\sigma}_{\mathrm{m}}(\nabla\cdot\mathbf{u})\mathbb{I} + \mathbf{S}(\mathbf{u}) \tag{2}$$

where the first term is defined by assuming that the mean stress, σ_{m}, only depends on the strain tensor trace ($\nabla\cdot\mathbf{u} = \operatorname{tr}(\boldsymbol{\varepsilon})$).

A classical widely used mixed variational approach to the mechanical quasi-static problem (1)–(2) is based on the set of primary variables $(p, \mathbf{u})$, where $p(\mathbf{x})$ is the negative mean stress (pressure). In this type of formulation, the stress field can be recovered by evaluating:

$$\boldsymbol{\sigma} = -p\mathbb{I} + \mathbf{S}(\mathbf{u}) \tag{3}$$

where p and $\mathbf{u}$ should verify the equation:

$$p = -\hat{\sigma}_{\mathrm{m}}(\nabla\cdot\mathbf{u}) \tag{4}$$

which can be considered as a continuum constraint between both proposed primary fields. We assume a linear relation of $\hat{\sigma}_{\mathrm{m}}$ with $\operatorname{tr}(\boldsymbol{\varepsilon})$, such as:

$$\hat{\sigma}_{\mathrm{m}}(\nabla\cdot\mathbf{u}) = \kappa\nabla\cdot\mathbf{u}; \quad \nabla\cdot\mathbf{u} = \hat{\sigma}_{\mathrm{m}}^{-1}(-p) = -\frac{p}{\kappa} \tag{5}$$

where κ is the bulk modulus ($\to\infty$ if the material is incompressible).

The variational equations of the mechanical problem (1)–(4) can be put in a classical mixed continuum format (see [15]): find $(p, \mathbf{u}) \in L_2(\Omega)\times H_1(\Omega)$, such that

$$\begin{aligned}\mathscr{L}([p,\mathbf{u}];[q,\mathbf{w}]) = &-\langle p, \nabla\cdot\mathbf{w}\rangle + \langle\mathbf{S}(\mathbf{u}), \nabla^s\mathbf{w}\rangle - \langle\rho\mathbf{b};\mathbf{w}\rangle \\ &- \int_{\Gamma_{\boldsymbol{\sigma}}} (\mathbf{t}\cdot\mathbf{w})\,\mathrm{d}\Gamma_{\boldsymbol{\sigma}} + \left\langle q, \left(\frac{p}{\kappa} + \nabla\cdot\mathbf{u}\right)\right\rangle = 0 \\ &\forall\mathbf{w}\in H_1^0(\Omega) \wedge \forall q\in L_2(\Omega)\end{aligned} \tag{6}$$

DOI: 10.1002/cnm

$\langle \cdot , \cdot \rangle$ being a duality product in Ω, the space $L_2(\Omega)$ includes the square integrable functions in Ω and $H_1(\Omega)$ includes the functions whose first derivatives are from $L_2(\Omega)$. We also call $H_1^0(\Omega)$ the sub-space of $H_1(\Omega)$ whose elements vanish in $\Gamma_{\mathbf{u}}$, the Dirichlet boundary of Ω.

2.1. Discrete stabilized variational form

Let $(p^h, \mathbf{u}^h)$, with $p^h \in Q \subset L_2(\Omega^h)$ and $\mathbf{u}^h \in \mathscr{V} \subset H_1(\Omega^h)$, be the finite element approaches of the above mentioned primary fields and $\mathscr{V}$ the finite element approach to $H_1(\Omega^h)$. Equal order of interpolations for those spaces could be introduced by the addition of stabilization terms $\mathscr{S}_{\text{st}}$. The discrete form of the problem reads:

$$\begin{aligned}\mathscr{L}([p^h, \mathbf{u}^h]; [q^h, \mathbf{w}^h]) = &-\langle p^h, \nabla \cdot \mathbf{w}^h \rangle + \langle \mathbf{S}(\mathbf{u}^h), \nabla^s \mathbf{w}^h \rangle - \langle \rho \mathbf{b}, \mathbf{w}^h \rangle \\ &- \int_{\Gamma_{\boldsymbol{\sigma}}} (\mathbf{t} \cdot \mathbf{w}^h)\, \mathrm{d}\Gamma_{\boldsymbol{\sigma}} + \left\langle q^h, \left(\frac{p^h}{\kappa} + \nabla \cdot \mathbf{u}^h \right) \right\rangle \\ &+ \mathscr{S}_{\text{st}}([p^h, \mathbf{u}^h]; [q^h, \mathbf{w}^h]) = 0 \quad \forall \mathbf{w}^h \in \mathscr{V}^0 \wedge \forall q^h \in Q \end{aligned} \tag{7}$$

Several different terms $\mathscr{S}_{\text{st}}$ have been proposed in the context of CFD. The GLS (Galerkin/least square) procedure [16] is probably the most known one. It has been extended to solid mechanics applications by Klass *et al.* [2], who have successfully used linear equal-order interpolations in large deformation incompressible elastic problems.

The pressure stabilizing Petrov–Galerkin (PSPG) scheme [17], which can be considered as a particular type of GLS procedure and the orthogonal sub-grid PGP method [12, 18] are shortly described in the following. The last scheme has been extended to the elastic solid mechanics context by Chiumenti *et al.* [3] and used in plasticity by Chiumenti *et al.* [4] and Cervera *et al.* [5] (see also [7]). These works show the plausibility of this approach in problems where alternative formulations hardly work well.

The above mentioned procedures consider the term $\mathscr{S}_{\text{st}}$ as being proportional to a stability factor τ depending on the elastic modulus and the finite element size, and therefore it changes from element to element.

2.2. PSPG stabilization procedure

The stabilization term $\mathscr{S}_{\text{st}}$ of Equation (7) is defined as follows:

$$\mathscr{S}_{\text{st}}^{\text{PSPG}} = -\left\langle \nabla q^h, \tau^{\text{PSPG}} \underbrace{(\nabla \cdot \boldsymbol{\sigma}(p^h, \mathbf{u}^h) + \rho \mathbf{b})}_{\mathbf{r}:\text{residue of the Cauchy equation}} \right\rangle \quad \forall q^h \in Q \tag{8}$$

where the factor τ^{PSPG} is:

$$\tau^{\text{PSPG}} = \alpha \frac{h^2}{2\mu} \tag{9}$$

α being a positive dimensionless parameter, h the element characteristic size and μ the shear modulus for the elastic problem.

DOI: 10.1002/cnm

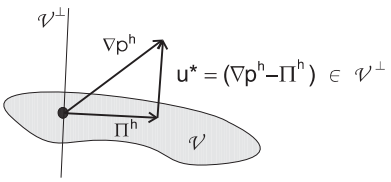

Figure 1. Pressure gradient projection.

Remark 1
Tezduyar *et al.* [17] have included in (7) an additional stabilization term for incompressibility constraint.

Remark 2
Klaas *et al.* [2] have considered a similar stabilization term without including the body force ($\rho\mathbf{b}$) in the **r** term of Equation (8). It has also been considered that, if dynamical problems are analysed, the inertial forces should be included in the same term, as it was initially proposed by Tezduyar *et al.* [17] in the CFD context.

2.3. PGP stabilization procedure

The stabilization term $\mathscr{S}_{\text{st}}$ is defined as follows:

$$\mathscr{S}_{\text{st}}^{\text{PGP}} = \langle \nabla q^h, \tau^{\text{PGP}}(\nabla p^h - \mathbf{\Pi}^h) \rangle \quad \forall q^h \in Q \tag{10}$$

where $\mathbf{\Pi}^h (\in \mathscr{V})$ is the L_2 projection of ∇p^h on $\mathscr{V}$ (see Figure 1):

$$\langle (\nabla p^h - \mathbf{\Pi}^h), \boldsymbol{\eta}^h \rangle = 0 \quad \forall \boldsymbol{\eta}^h \in \mathscr{V} \tag{11}$$

We remark that functions in $\mathscr{V}$ do not vanish on $\Gamma_{\mathbf{u}}^h$, thus, $\mathbf{\Pi}^h$ is a vector field in $\mathbb{R}^n$ lying in the same finite element space of $\mathbf{u}^h$. Equation (11), which determines the '*PGP*' field $\mathbf{\Pi}^h$, should be added to the mixed variational form (7).

The stabilization parameter τ^{PGP} can be determined elementwise as a function of the element characteristic size and the shear modulus:

$$\tau^{\text{PGP}} = c\frac{h^2}{2\mu^*} \tag{12}$$

where the scalar coefficient $c = 4$ has been employed by Codina [12] in CFD application problems. Following Chiumenti *et al.* [4], we have adopted the secant shear modulus μ^* in the $J2$ plasticity problems.

3. NUMERICAL IMPLEMENTATION OF THE PGP STABILIZATION SCHEME

We approach the variational formulation (7) by using the PGP stabilization term (10) with the projection (11) being included as an additional equation.

DOI: 10.1002/cnm

Let a finite element method using equal-order interpolation fields for Q and $\mathscr{V}$ (particularly $\mathscr{C}^0$ linear approaches) be considered. The mechanical problem can be rewritten in the following terms: determine $p \in Q$ and $\mathbf{u} \in \mathscr{V}$, such that (here we remove the superscript h)

$$-\langle p, \nabla \cdot \mathbf{w} \rangle + \langle \mathbf{S}(\mathbf{u}), \nabla^s \mathbf{w} \rangle - \langle \rho \mathbf{b}, \mathbf{w} \rangle = \int_{\Gamma_\sigma} (\mathbf{t} \cdot \mathbf{w}) \, \mathrm{d}\Gamma_\sigma \quad \forall \mathbf{w} \in \mathscr{V}^0 \tag{13}$$

$$\left\langle q, \left(\frac{p}{\kappa} + \nabla \cdot \mathbf{u} \right) \right\rangle + \langle \nabla q, \tau^{\mathrm{PGP}} (\nabla p - \mathbf{\Pi}) \rangle = 0 \quad \forall q \in Q \tag{14}$$

$$\langle (\nabla p - \mathbf{\Pi}), \boldsymbol{\eta} \rangle = 0 \quad \forall \boldsymbol{\eta} \in \mathscr{V} \tag{15}$$

Introducing some of standard matrix notations, the interpolated fields can be expressed as:

$$\mathbf{u}(\mathbf{x}, t) = \mathbf{N}_\mathbf{u}(\mathbf{x}) \hat{\mathbf{u}}(t), \quad \mathbf{w}(\mathbf{x}) = \mathbf{N}_\mathbf{u}(\mathbf{x}) \hat{\mathbf{w}} \tag{16}$$

$$p(\mathbf{x}, t) = \mathbf{N}_p(\mathbf{x}) \hat{\mathbf{p}}(t), \quad q(\mathbf{x}) = \mathbf{N}_p(\mathbf{x}) \hat{\mathbf{q}} \tag{17}$$

$$\mathbf{\Pi}(\mathbf{x}, t) = \mathbf{N}_\mathbf{u}(\mathbf{x}) \hat{\mathbf{\Pi}}(t), \quad \boldsymbol{\eta}(\mathbf{x}) = \mathbf{N}_\mathbf{u}(\mathbf{x}) \hat{\boldsymbol{\eta}} \tag{18}$$

where $\mathbf{N}_u$ and $\mathbf{N}_p$ are the shape function matrices and the symbol $(\hat{\cdot})$ refers to the interpolation parameters. Furthermore, let:

$$\nabla^s \mathbf{N}_\mathbf{u} = \mathbf{B} \tag{19}$$

$$\nabla \cdot \mathbf{N}_\mathbf{u} = \mathbb{I}^{\mathrm{T}} \mathbf{B} \tag{20}$$

$$\nabla \mathbf{N}_p = \mathbf{D} \tag{21}$$

where $\mathbf{B}$ is the standard strain–displacement matrix and $\mathbb{I}$ the vector representation of the second order identity tensor.

The matrical form of Equations (13)–(15) can be written as:

$$\begin{aligned} &\mathop{\mathsf{A}}_{e=1}^{nel} \left[\int_{\Omega^e} \mathbf{B}^{\mathrm{T}} \mathbf{S}(\hat{\mathbf{u}}) \, \mathrm{d}\Omega^e \right] - \mathbf{G}_0 \hat{\mathbf{p}} = \mathbf{f} \\ &-\mathbf{G}_0^{\mathrm{T}} \hat{\mathbf{u}} - \left[\frac{1}{\kappa} \mathbf{M}_p + \mathbf{L} \right] \hat{\mathbf{p}} + \mathbf{H}^{\mathrm{T}} \hat{\mathbf{\Pi}} = \mathbf{0} \\ &\mathbf{H} \hat{\mathbf{p}} - \mathbf{M}_\mathbf{u} \hat{\mathbf{\Pi}} = \mathbf{0} \end{aligned} \tag{22}$$

A being the standard finite element assembly operator. The sign of equation (22b) has been changed and (22c) scaled by τ^{PGP} to evidence the symmetry of the discrete system. The vector $\mathbf{f}$ is considered as the discrete external force, and the matrices $\mathbf{G}_0$, $\mathbf{M}_p$, $\mathbf{M}_\mathbf{u}$, $\mathbf{L}$ and $\mathbf{H}$ are defined as:

$$\mathbf{G}_0 = \mathop{\mathsf{A}}_{e=1}^{nel} \left[\int_{\Omega^e} \mathbf{B}^{\mathrm{T}} \mathbb{I} \mathbf{N}_p \, \mathrm{d}\Omega^e \right] \tag{23}$$

DOI: 10.1002/cnm

$$\mathbf{M}_p = \mathop{\mathsf{A}}_{e=1}^{nel} \left[\int_{\Omega^e} \mathbf{N}_p^{\mathrm{T}} \mathbf{N}_p \, \mathrm{d}\Omega^e \right] \tag{24}$$

$$\mathbf{M}_{\mathbf{u}} = \mathop{\mathsf{A}}_{e=1}^{nel} \left[\int_{\Omega^e} \mathbf{N}_{\mathbf{u}}^{\mathrm{T}} \tau^{\mathrm{PGP}} \mathbf{N}_{\mathbf{u}} \, \mathrm{d}\Omega^e \right] \tag{25}$$

$$\mathbf{L} = \mathop{\mathsf{A}}_{e=1}^{nel} \left[\int_{\Omega^e} \mathbf{D}^{\mathrm{T}} \tau^{\mathrm{PGP}} \mathbf{D} \, \mathrm{d}\Omega^e \right] \tag{26}$$

$$\mathbf{H} = \mathop{\mathsf{A}}_{e=1}^{nel} \left[\int_{\Omega^e} \mathbf{N}_{\mathbf{u}}^{\mathrm{T}} \tau^{\mathrm{PGP}} \mathbf{D} \, \mathrm{d}\Omega^e \right] \tag{27}$$

where the subscript 0 accounts for the Dirichlet homogeneous boundary condition on the displacement variational space $\mathscr{V}^0$.

The algebraic non-linear system of Equations (22), which depends on the pseudo-time (t), can be solved for every load step by a standard Newton–Raphson procedure. In this case, the high computational cost, due to the introduction of the new field $\mathbf{\Pi}$, provides a no competitive scheme if compared with stabilized alternative stategies. Following Codina [12] and Chiumenti *et al.* [3], a simplified treatment can be introduced to make it more efficient. Considering that the PGP field $\mathbf{\Pi}$ does not change significantly between the ith and the $(i+1)$th load step, it is possible to solve the alternative equation system:

$$\begin{aligned} &\mathop{\mathsf{A}}_{e=1}^{nel} \left[\int_{\Omega^e} \mathbf{B}^{\mathrm{T}} \mathbf{S}_{(i+1)} \, \mathrm{d}\Omega^e \right] - \mathbf{G}_0 \hat{\mathbf{p}}_{(i+1)} = \mathbf{f}_{(i+1)} \\ &-\mathbf{G}_0^{\mathrm{T}} \hat{\mathbf{u}}_{(i+1)} - \left[\frac{1}{\kappa} \mathbf{M}_p + \mathbf{L}_{(i+1)} \right] \hat{\mathbf{p}}_{(i+1)} = -\mathbf{H}_{(i+1)}^{\mathrm{T}} \hat{\mathbf{\Pi}}_{(i)} \end{aligned} \tag{28}$$

where $\hat{\mathbf{\Pi}}_{(i)}$ is evaluated, by considering Equation (22c), once the nonlinear solver has converged for displacement and pressure variables at the ith load step. At the global level, it is possible to express:

$$\hat{\mathbf{\Pi}}_{(i)} = \mathbf{M}_{\mathbf{u}}^{-1} \mathbf{H}_{(i)} \hat{\mathbf{p}}_{(i)} \tag{29}$$

Therefore, the right-hand side term of (28b) can be considered as an external force for this equation, while the evaluation of $\hat{\mathbf{\Pi}}_{(i)}$, from Equation (29) at the end of the ith step, requires the same computational cost as a smoothing of the displacement field.

3.1. Parallel implementation

This formulation has been implemented in the PETSc-FEM code [13]. It is a general purpose multiphysics finite element program developed at the International Center of Computational Methods in Engineering (CIMEC) running on a Beowulf cluster. PETSc-FEM makes use of the portable, extensible toolkit for scientific computation (PETSc) library [19–21] for linear algebra operations, MPI libraries [22] as the communication package and C++ object-oriented philosophy. PETSc-FEM is a library and a set of applications which can be used to solve the incompressible Navier–Stokes

DOI: 10.1002/cnm

equations, the compressible Euler equations, shallow water model, general advective–diffusive systems, Laplace equation and solid mechanics problems.

The PETSc library allows to treat vectors and matrices in a distributed memory environment. Therefore, it performs the allocation of data on the nodes of the cluster and allows the user to make calls to sub-routines for linear algebra, including linear equation system solvers, without dealing explicitly with parallelism. Mesh partitioning in PETSc-FEM is performed by using METIS [23].

In the solution of the linear equation system and within the parallel implementation context, iterative techniques should be used, in general, by efficiency considerations. Furthermore, for this algorithmic stage and as a consequence of the PGP stabilization procedure, the resulting global system of equations is symmetric but not positive definite, which constraints us to use a limited number of solution schemes. We make use of two strategies, a global iterative scheme and a domain decomposition method (DDM):

- The global iterative GMRES scheme (GGMRES) is performed in parallel to solve the full linear system of equations.
- The DDM has been found to behave better than global iterative methods, specially for large and bad conditioned problems [14]. It is based on decomposing the whole domain into sub-domains in such a way that solving the global system may be split into two phases: solving internal sub-domain unknowns and solving global interface unknowns. The internal unknowns may be solved concurrently on each computing node by direct methods (based on LU strategy (lower and upper block triangular matrix decomposition)). The interface unknowns make part of a global reduced system which is solved by means of iterative methods (a GMRES-based scheme could be used in this step). In what follows, this technique will be denoted as Interface–Iterative/Sub domain-Direct (IISD) method.

  Decomposing the domain into non-overlapping sub-domains leads to the interface problem whose matrix is the Schur complement. The size of the global interface system is much smaller than that of the global system. In order to improve the computational efficiency, this interface solver must be preconditioned so as to reduce the condition number of the Schur complement matrix. We use an interface strip (IS) preconditioner recently developed by Storti *et al.* [14].

  The IS preconditioner requires less memory and computational cost than classical Neumann–Neumann preconditioner and its variants. In this work, the application of IISD/IS preconditioner has been extended to the solid mechanics context.

Memory requirements for both strategies increase when the solution error tolerance decreases. The DDM needs more memory resources than the global iterative procedure with coarse tolerances. However, when decreasing tolerance, the memory growth rate is higher for the global iterative

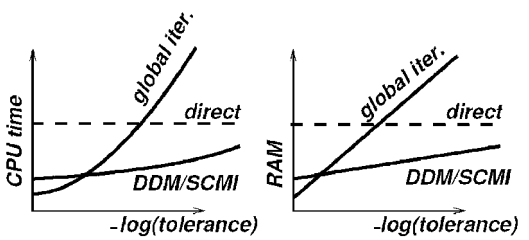

Figure 2. Memory (RAM) and processing time requirements (CPU time) for different solvers. DDM/SCMI: Domain Decomposition Method with Schur Complement Matrix Interface.

DOI: 10.1002/cnm

strategy (see Figure 2). Therefore, DDM is more efficient when tight tolerances are required, as was found in some practical problems [14].

The introduction of the stabilized mixed formulation does not change the structure of the above-mentioned algorithm for parallelization.

4. NUMERICAL TESTS

The numerical performance of the linear–linear PGP stabilization method is evaluated for 2D and 3D tests and is compared with that shown by the standard Galerkin (STD), the standard P1–P1 mixed formulation without stabilization terms (MSTD) and the PSPG stabilization scheme.

The first test is a convergence study of the $(p, \mathbf{u})$ fields with mesh refinement, when compressible or incompressible elastic problems are considered. This example also validates the model in terms of an analytical solution.

Section 4.2 presents a problem involving a large number of unknowns that is computed in parallel mode. The above mentioned iterative strategies and its numerical performances are compared.

The following Sections 4.3–4.5, are devoted to the solution of plasticity problems. We are particularly interested in analysing the PGP formulation capability for capturing the limit load, collapse mechanisms and mesh independence postcritical response. The last property becomes one of the most important finite element characteristic for obtaining correct slip line representation arising as a typical phenomenon in failure prediction modelling.

4.1. Convergence analysis

In the first place, an elastic problem with analytical solution, consisting of a plane strain cantilever beam subjected to a flexure deformation mode, is considered (we take this example from [24]).

Figure 3(a) shows the physical model, the geometry and the external loads. The analytical displacement field is:

$$u_x(x, y) = \frac{Fy}{6\overline{E}I}\left[(6L - 3x)x + (2 + \overline{\nu})\left(y^2 - \frac{1}{4}D^2\right)\right]$$

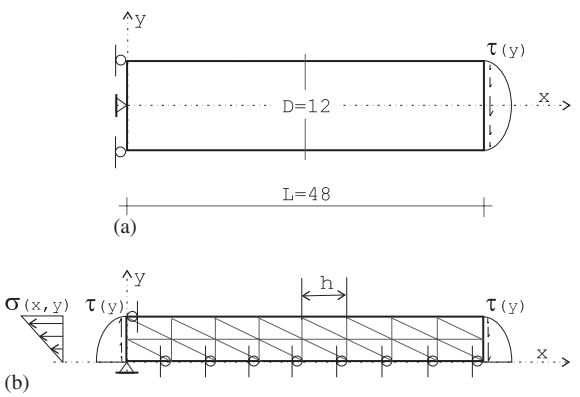

Figure 3. Cantilever flexion test: (a) geometry and (b) numerical model.

DOI: 10.1002/cnm

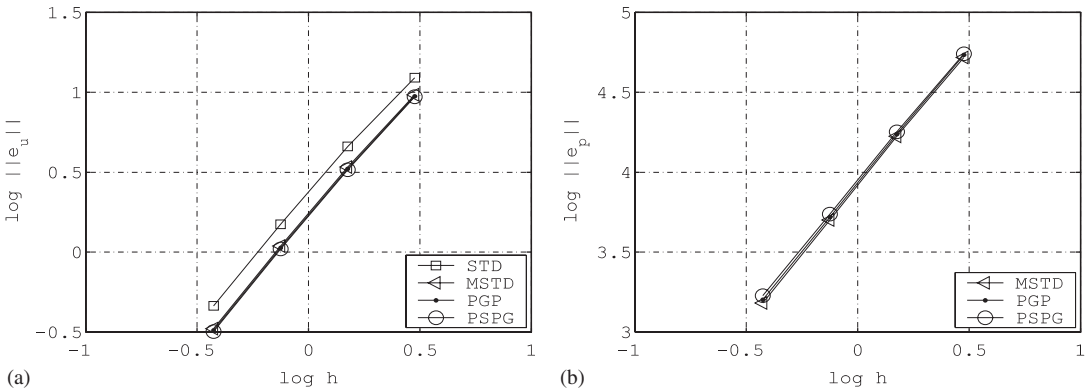

Figure 4. Compressible case $v = 0.25$: (a) displacement and (b) pressure.

$$u_y(x, y) = -\frac{F}{6\overline{E}I}\left[3\overline{v}y^2(L-x) + \frac{1}{4}(4+5\overline{v})D^2x + (3L-x)x^2\right] \tag{30}$$

where F is the resultant tangential load, $I = D^3/12$, $\overline{E} = E/(1-v^2)$ and $\overline{v} = v/(1-v)$, with E and v the Young's modulus and Poisson's ratio, respectively.

The traction boundary condition should be imposed in such a way that they be compatible with the stress field analytical solution. At $x = 0$, they are:

$$\begin{aligned} \sigma_x(0, y) &= -\frac{Fy}{I}L \\ \tau_{xy}(y) &= \frac{F}{2I}\left[\frac{1}{4}D^2 - y^2\right] \end{aligned} \tag{31}$$

And at $x = L$, $\sigma_x = \sigma_y = 0$ and the shear stress is given by (31b).

Figure 3(b) depicts the kinematical and mechanical boundary conditions for the coarsest mesh (only the top half part of the beam is modelled). Four element size are considered, all of them using an aspect ratio of 2.

The convergence analysis is carried out in terms of displacement and pressure error measures (e_u, e_p), according to the L_2-norm computed as:

$$\|e_u\|_{L_2(\Omega)} = \|(\mathbf{u}_{\mathrm{EX}} - \mathbf{u}_{\mathrm{EF}})\|_{L_2(\Omega)} = \left[\int_\Omega (\mathbf{u}_{\mathrm{EX}} - \mathbf{u}_{\mathrm{EF}})^2 \, \mathrm{d}\Omega\right]^{1/2} \tag{32}$$

where $\mathbf{u}_{\mathrm{EX}}$ and $\mathbf{u}_{\mathrm{EF}}$ represent the exact and numerical displacement solutions respectively.

Two situations are analysed in terms of v coefficient ($v = 0.25$ and 0.49999). Figures 4 and 5 show the convergence curves of standard (STD), mixed (MSTD) and both mixed stabilized PGP and PSPG (with $c = 1$ and $\tau^{\mathrm{PGP}} = \tau^{\mathrm{PSPG}}$) triangles as a function of the characteristic element size h.

Note that in the compressible situation, the four FE formulations show similar convergence rates, in displacement and also in pressure. In this case both, the PGP and PSPG, strategies are clearly unfavourable from the computational point of view. However, in the incompressible regime,

DOI: 10.1002/cnm

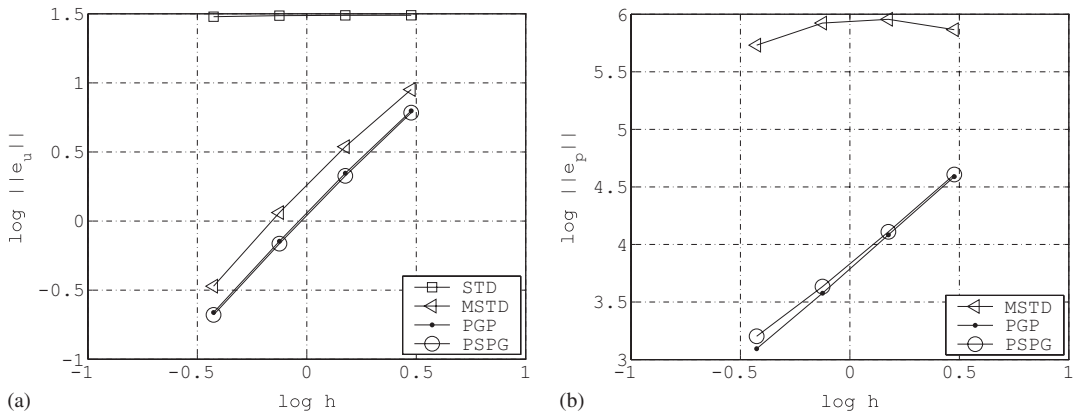

Figure 5. Incompressible case $v = 0.49999$: (a) displacement and (b) pressure.

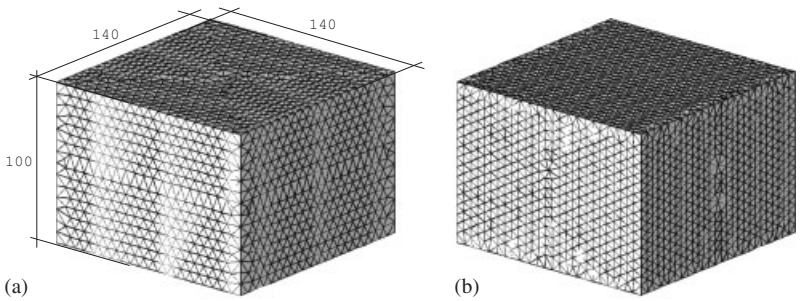

Figure 6. Elastic block: FE meshes: (a) 56 000 and (b) 90 000 tetrahedral elements.

a convergence rate of approximately 1.7 (for displacement and pressure) is obtained for the PGP and PSPG elements, similar to that obtained in the compressible regime. This means that the incompressibility constraint does not affect the convergence rates of the interpolated fields as it happens with the other formulations.

4.2. Incompressible elasticity

We consider a nearly incompressible elastic block of $140 \times 140 \times 100$ (unit length in millimetres) subjected to the following boundary conditions: all displacement are prescribed to zero at the bottom surface, the top surface is glued to a stiff plate imposing a vertical downward displacements ($\delta_y = 7$ mm); the lateral faces are free. The mechanical parameters are: Young's modulus $E = 2\,999\,800$ MPa, Poisson's ratio $v = 0.4999$.

Figure 6 shows the discrete models for two unstructured meshes of about 56 000 (Figure 6(a)) and 90 000 (Figure 6(b)) tetrahedral elements. To test the numerical performance of the parallel implementation, this example has been computed solving simultaneously the fully coupled system of Equations (22) (entailing approximately 71 000 and 112 000 equations, respectively). This monolithic scheme provides a more challenging test for the iterative solver of the linear equation system.

DOI: 10.1002/cnm

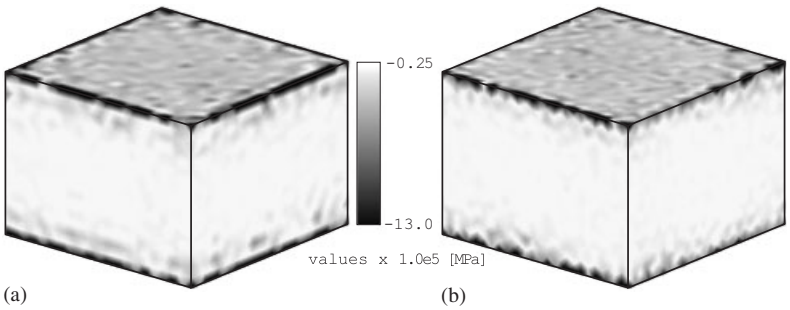

Figure 7. Mean stress maps, MSTD formulation: (a) 56 000 and (b) 90 000 elements.

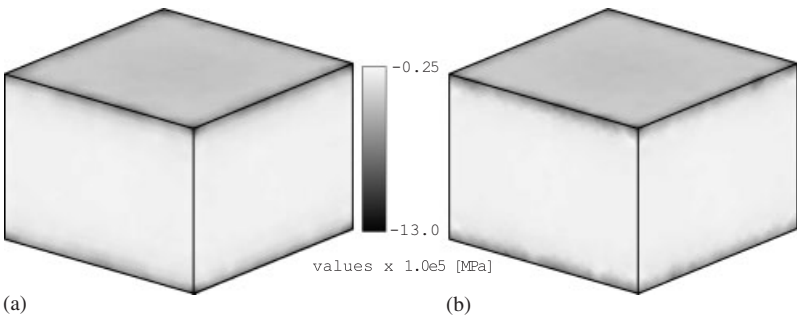

Figure 8. Mean stress maps, PGP formulation: (a) 56 000 and (b) 90 000 elements.

Figure 7 shows the mean stress field for both meshes and assuming a negligible level of stabilization ($c \approx 0$). This situation represents the response of an unstable mixed standard formulation (MSTD). Severe locking effects can be observed. The mean stress oscillation diminishes drastically if the stabilization term $\mathscr{S}_{\text{st}}^{\text{PGP}}$ is activated, as can be seen in Figure 8, where $c = 1$ has been considered.

The transition from unstable to stable solution by varying the c parameter can be more clearly evidenced in Figure 9, where the mean stress distributions along the internal line $\overline{AB}$ have been plotted for different values of c.

Figure 10 displays a comparison between the mean stress curves along the $\overline{AB}$ internal line for the PSPG and PGP stabilization schemes. It can be observed that both solutions are practically identical. According to expressions (9) and (12), the stabilization factors that have been used in this simulation are:

$$\tau^{\text{PSPG}} = \frac{h^2}{12\mu}, \quad \tau^{\text{PGP}} = \frac{2h^2}{\mu} \tag{33}$$

Next, we examine the numerical performance of the parallel implementation procedures. Nine nodes of a PC cluster (P4, 2.4 GHz, 1 GB RAM DDR 333 MHz) were utilized. The comparative analysis of the computational cost for solving the monolithic system of equations, without uncoupling

DOI: 10.1002/cnm

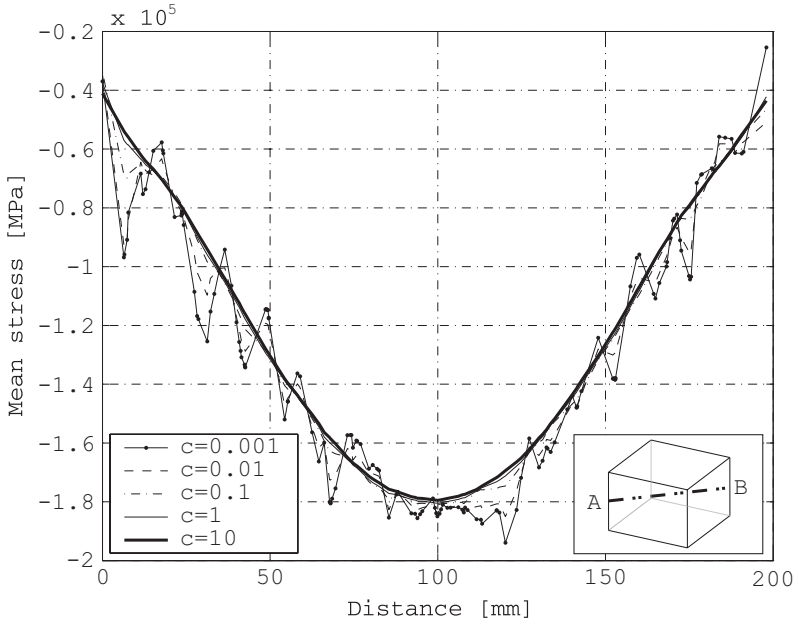

Figure 9. Mean stress curves along of $\overline{AB}$ line, PGP formulation.

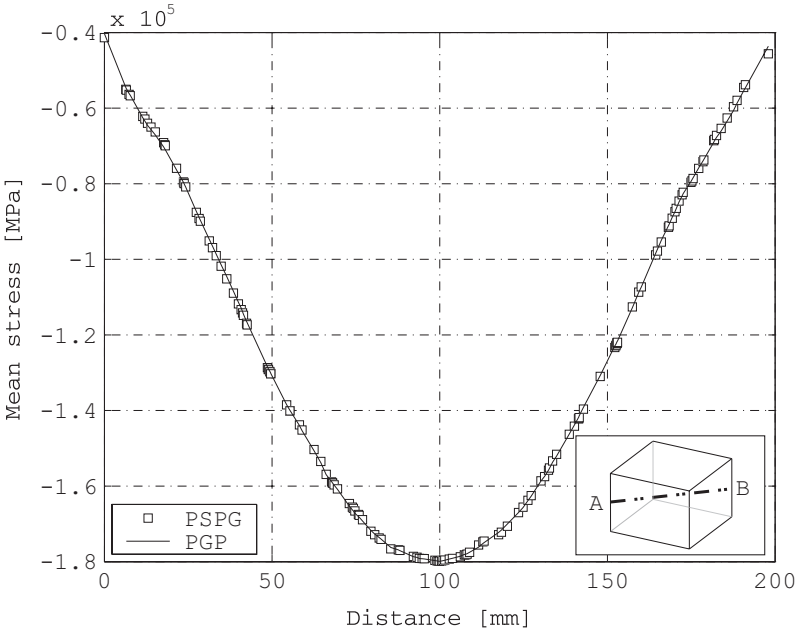

Figure 10. Stabilization procedure comparison: PSPG *vs* PGP.

DOI: 10.1002/cnm

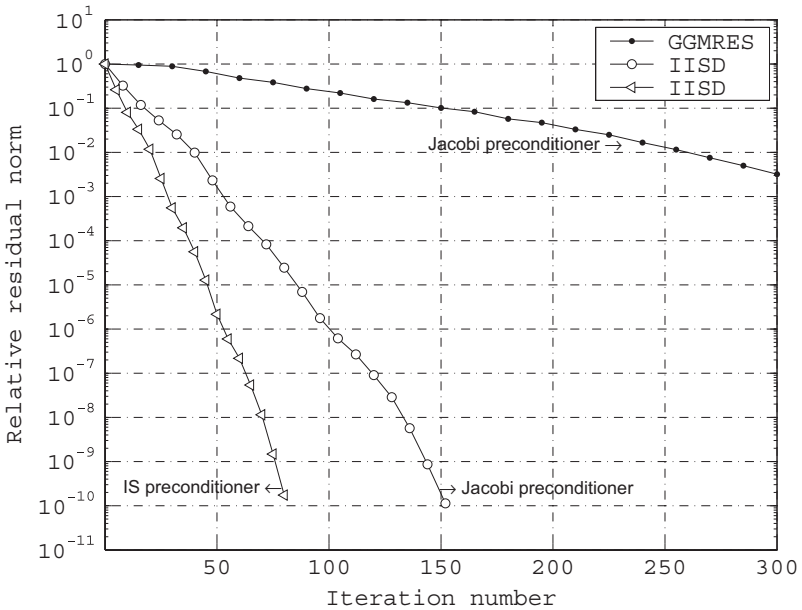

Figure 11. Linear solver convergence, test with 90 000 elements.

Table I. Time performance, test with 56 000 elements.

Solver strategy	Preconditioner	Absolute time (s)	Relative time
GGMRES	Jacobi	64.85	3.33
IISD	Jacobi	19.47	1.00
IISD	IS	16.93	0.87

the **Π** field, considers the two strategies mentioned above (Section 3.1):

- The global iterative GMRES scheme (GGMRES), where the iterative process is carried out in parallel, using the standard Jacobi preconditioner.
- The IISD (based on DDM) technique, where the whole domain is decomposed on nine subdomains, each one is allocated on a cluster-processing node, and both preconditioners, the standard Jacobi and the IS, are compared in the simulations.

Figure 11 depicts, for the 90 000 element test, the required number of iterations to reduce 10 orders of magnitude the relative error of the residual norm. The differences between the IISD and GGMRES strategies are evident, see also Tables I and II.

In the IISD context, less iterations are needed when using the IS preconditioner with respect to the Jacobi one, and consequently, less memory is required to store the Krylov space. Less number of iterations does not imply, by itself, better performance of the algorithm. Nevertheless, the computing time given in Tables I and II shows that the IS preconditioner behaves better than the Jacobi, with an improvement of approximately 12%, for these problems. Even when efficient

DOI: 10.1002/cnm

Table II. Time performance, test with 90 000 elements.

Solver strategy	Preconditioner	Absolute time (s)	Relative time
GGMRES	Jacobi	197.02	3.83
IISD	Jacobi	51.49	1.00
IISD	IS	45.99	0.89

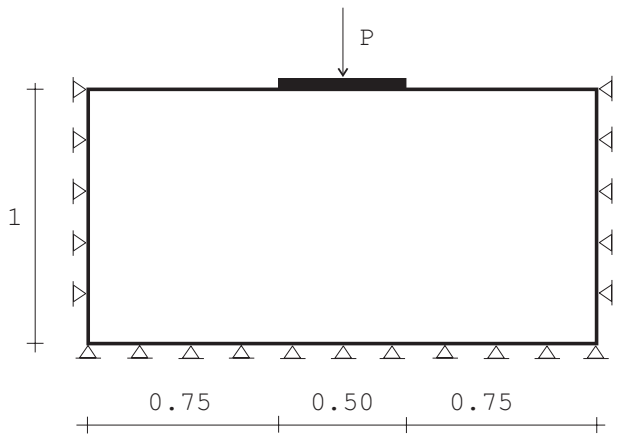

Figure 12. Geometry and boundary condition for 2D plane strain Prandtl test.

implementation of the IS preconditioner is, at the present, under development, it should be remarked that this procedure shows promising results.

4.3. 2D Prandtl test

The objective of this numerical application, which corresponds to the 2D plane strain version of the Prandtl's punch test, is to evaluate the response sensitivity, particularly in the limit load and the collapse mechanism, with respect to the finite element mesh orientation. The solution is given by analysing specially designed mesh configurations to challenge the present formulation.

The classical problem consists of a semi-infinite half space vertically loaded by a stiff plate. We have limited the studied domain to a rectangular zone as shown in Figure 12 (dimensions in millimetres).

The (non-unique) collapse mechanism and the corresponding (unique) structural limit load, considering a J2 elastic-perfectly plastic material, has been determined analytically (see, for example, [25, p. 219]). The limit load solution is $\sigma_N/\sigma_y = (2+\pi)/\sqrt{3}$, where σ_N is the nominal stress under the punch and σ_y the material yield stress. In the present test, the punch displacement is constrained to move without rotation, inducing a unique (symmetric) solution for the collapse mechanism.

Figure 13 shows two finite element discretizations. The first configuration (Figure 13(a)) displays a (closely) *symmetrical* distribution of elements and nodes. The second one represents a *biased* mesh (Figure 13(b)), specially designed to evidence a directional mesh orientation '*d*' coinciding, very aproximately, with one of the slip line directions of the collapse mechanisms

DOI: 10.1002/cnm

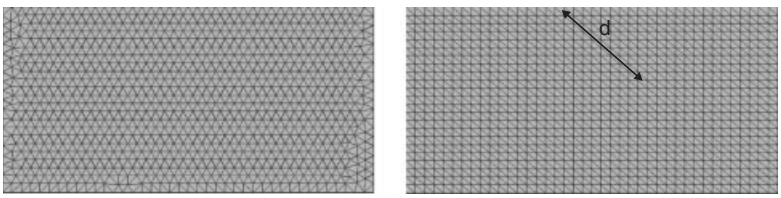

Figure 13. Mesh configurations: (a) symmetrical mesh and (b) biased mesh.

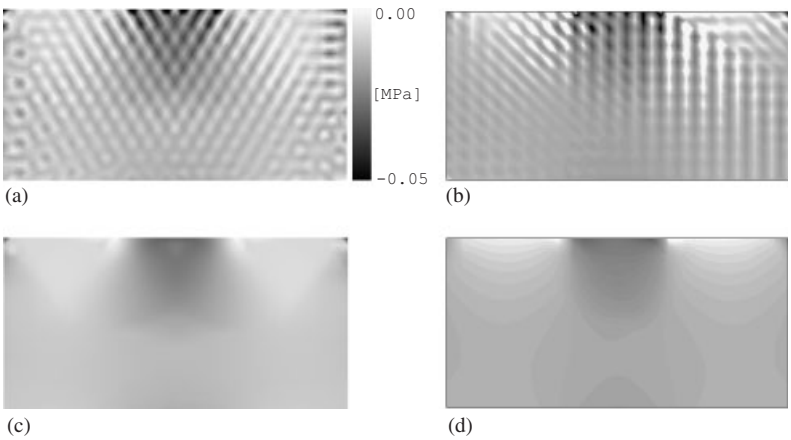

Figure 14. Mean stress maps: (a) MSTD formulation, symmetrical mesh; (b) MSTD formulation, biased mesh; (c) PGP formulation, symmetrical mesh; and (d) PGP formulation, biased mesh.

predicted by the analytical solution. Both of them have approximately 1800 triangular elements. The material properties are: Young's modulus $E = 1.0$ MPa, Poisson's ratio $v = 0.499$ (observe the quasi-incompressible elastic response considered here), yield stress $\sigma_y = 0.01$ MPa, perfectly plastic von Mises constitutive model.

Both, the *symmetrical* and the *biased* configuration, have been solved using the mixed triangle with the PGP stabilization procedure ($c = 1$) and the standard mixed triangle MSTD ($c \approx 0$). The mean stress values, at plastic regime, are displayed in Figure 14. Again, the standard mixed formulation shows a poor performance characterized by a severe oscillation in the mean stress field, while the PGP formulation gives a smooth solution.

The capturing of the collapse mechanism for both meshes are analysed in Figure 15. It shows the equivalent plastic strain fields once the plastic flow is fully achieved. In agreement with the analytical solution, we can observe that for the PGP formulation and the symmetrical mesh, the failure mechanism is in correspondence with the expected symmetrical slip line pattern (Figure 15(a)). Nevertheless, the PGP formulation with a biased mesh does not present a symmetrical distribution of this field. This feature is much more marked in the solution obtained by using the STD triangle with the biased configuration, Figure 15(c). The same behaviour about the resulting symmetry loss can be observed by analysing the displacement field. Figure 16 shows the

DOI: 10.1002/cnm

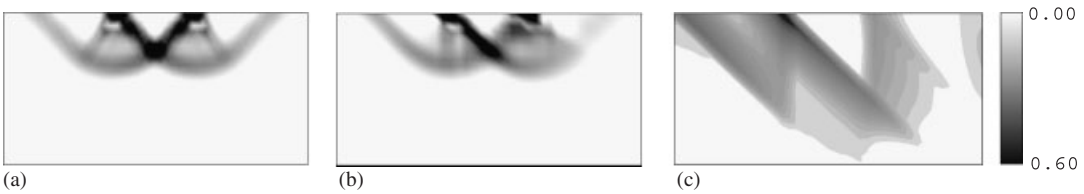

Figure 15. Equivalent plastic strain maps: (a) PGP symmetrical mesh; (b) PGP biased mesh; and (c) STD biased mesh.

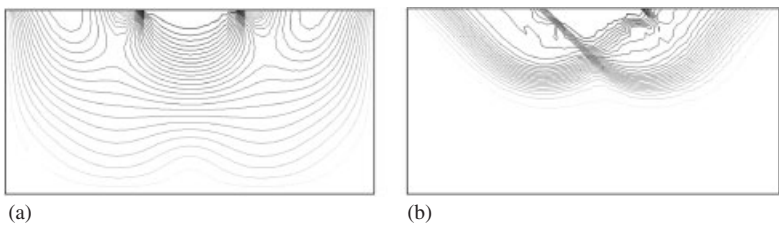

Figure 16. Iso-displacement contour lines: (a) PGP biased mesh in the elastic regime and (b) PGP biased mesh in the fully plastic regime.

iso-displacement curves for the PGP model with the biased mesh configuration. During the elastic regime (Figure 16(a)), even considering elastic incompressibility, the displacement field is very approximately symmetrical. However, once the concentration of the plastic deformations begins, this feature is lost (Figure 16(b)). A similar study in the STD triangle shows that the symmetry loss is produced when isochoric deformations are modelled, independently of the plastic flow presence. We can conclude that this phenomenon, the symmetry loss of results, is caused by the well-known finite element limitation to capture some type of kinematical constraints. Nevertheless, these deficiencies are much less marked in the PGP formulation with respect to the STD one. In any case, some mesh dependence behaviour is observed.

Figure 17 compares the total plate reaction *vs* the vertical plate displacement curves for both meshes with different alternatives: the standard Galerkin (STD), the standard mixed (MSTD) and the stabilized mixed (PGP) formulations. As it is expected, the standard Galerkin element shows a response without limit load, while the MSTD and PGP formulations, either for symmetrical or biased meshes, show a well-defined limit load. A mesh refining and a larger domain of analysis shall give a more adjusted prediction of the analytical solution. It is observed that the limit load predictions are in good agreement with the analytical solution for both mesh configurations.

Table III shows the comparative computational cost, running in one processor, introduced by the mixed stabilized formulation (PGP) with respect to the standard finite element formulation and for different parts of the numerical process. The figure of the total CPU cost, in the first column, compares well with that reported in Reference [5].

We remark that the $\mathbf{\Pi}$ field evaluation, when using the procedure described in (28) and (29), shows a small computational cost in comparison with other part of the algorithm ($<5\%$ than that required by the system solution).

DOI: 10.1002/cnm

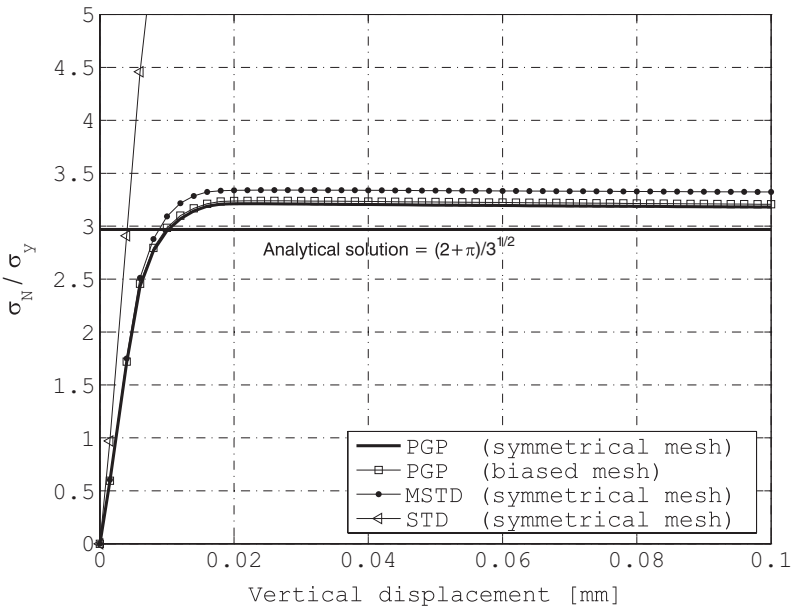

Figure 17. Load–displacement curve.

Table III. 2D Prandtl test, computing time values (CPU) for the PGP method relative to the standard STD triangle.

Total	Stiffness matrix	System solution	Internal forces
1.73	1.81	2.61	1.22

4.4. 3D notched cylinder

This example is devoted to study the behaviour of tetrahedral stabilized PGP elements under severe plastic strain state. It is a cylindrical notched specimen under axial tension by application of incremental displacements. The geometry proportions and the discrete model (of about 7800 elements), used in the simulation, can be seen in Figure 18 (due to symmetry conditions only $\frac{1}{8}$ of the bar is discretized). The following mechanical properties have been assumed: Young's modulus $E = 3 \times 10^3$ MPa, Poisson's ratio $v = 0.3$, and a J2 perfectly plastic model with yield stress $\sigma_y = 50$ MPa.

Figure 19 shows the normalized nominal stress (σ_N/σ_y) *vs* normalized imposed displacement ($E\delta_y/(W\sigma_y)$) curves for two different finite element formulations. The irreducible standard Galerkin model (STD) fails again to capture a limit load. The PGP stabilized element (with $c \approx 1$), instead, exhibits a well-defined limit structural strength. The limit load determination in this example is equivalent to the limit load problem of the punch test. However, the authors do not know an analytical solution for it when considering the symmetry of revolution and von Mises yield criteria.

DOI: 10.1002/cnm

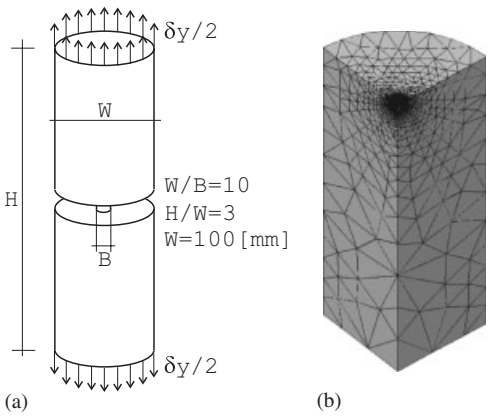

Figure 18. 3D notched cylinder problem: (a) geometry and (b) discrete model.

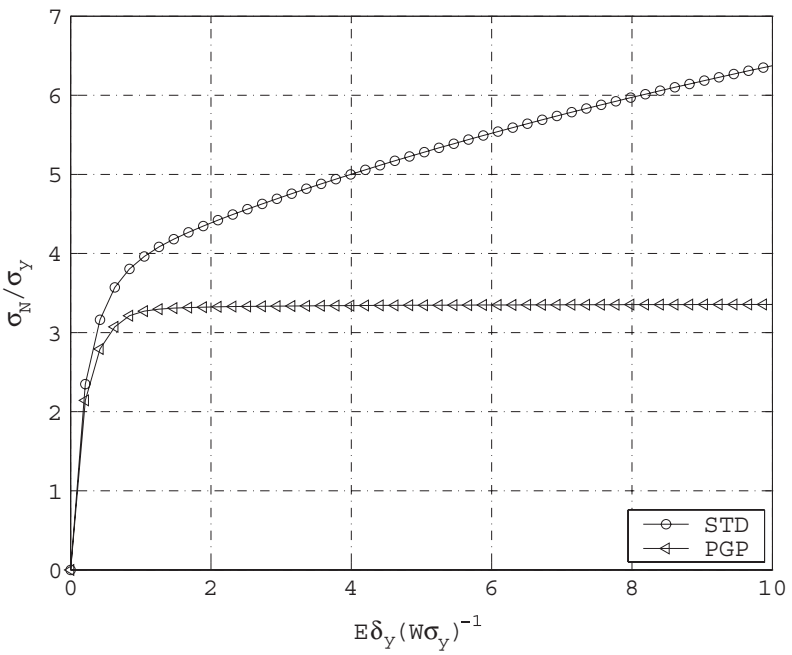

Figure 19. Load–displacement curve.

Figure 20 depicts the mean stress field, close to the notched zone in correspondence with the last load step. In this case, two situations in terms of c parameter are considered: by choosing $c = 0.04$, the stabilization effect is practically neglected, while $c = 4$ imposes an important stabilization effect. Again, the stabilization influence to avoid spurious oscillation modes is noticeable.

For the solution with $c = 4$ and once the fully plastic regimen was achieved, Figure 21 displays the vertical displacement map and the equivalent plastic strain field in that zones close to the notch.

DOI: 10.1002/cnm

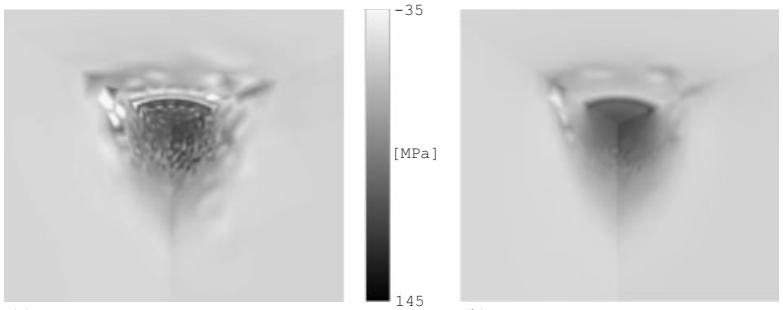

Figure 20. Mean stress maps, PGP formulation: (a) $c = 0.04$ and (b) $c = 4$.

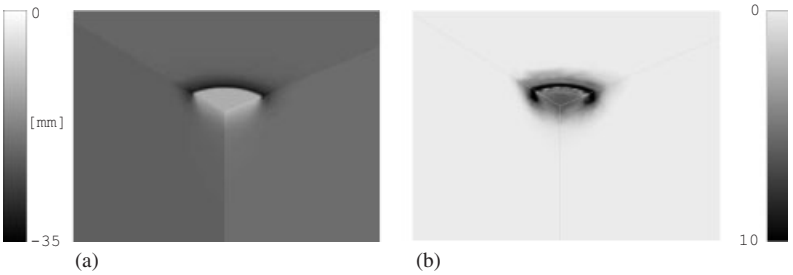

Figure 21. Contour fills, $c = 4$: (a) vertical displacements and (b) equivalent plastic strain.

4.5. Localization problem

A compression test of a prismatic square section block, under plain strain assumption, is analysed. This numerical example has been previously used by some authors at the beginning of 1990s to test the ability of finite element formulations for modelling strain localization problems. J2 elasto-plastic material model with linear softening is adopted. Under this condition and after the material instability critical condition has been reached, the development of a plastic strain localization zone is expected (with an inclination of about 45°). We analyse the capability of the stabilized PGP triangle to capture this failure mechanism.

Figure 22(a) shows the geometric proportions of the problem (dimensions in millimetres). A quarter of the block is considered in the numerical simulation (see Figure 22(b)). The mechanical parameters are: Young's modulus $E = 3 \times 10^4$ MPa, Poisson's ratio $\nu = 0.3$, yield stress $\sigma_y = 36$ MPa, softening material modulus $H = -1.8 \times 10^3$ MPa.

The constitutive model has not been regularized with the finite element size. Therefore, the computed load–displacement curve will change with mesh refinement. However, our interest here is to show the mesh direction sensibility rather than the mesh size independence. It should be expected that by using different meshes, with similar element size, the results should be comparable even if the mesh direction changes.

DOI: 10.1002/cnm

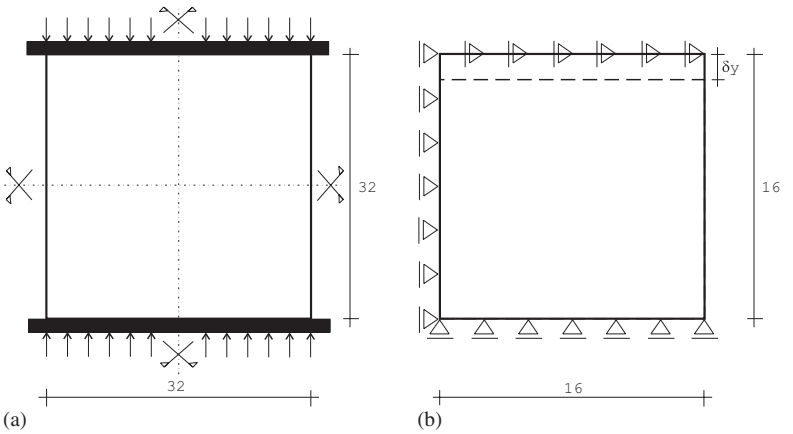

Figure 22. Localization problem: (a) physical model and (b) numerical model.

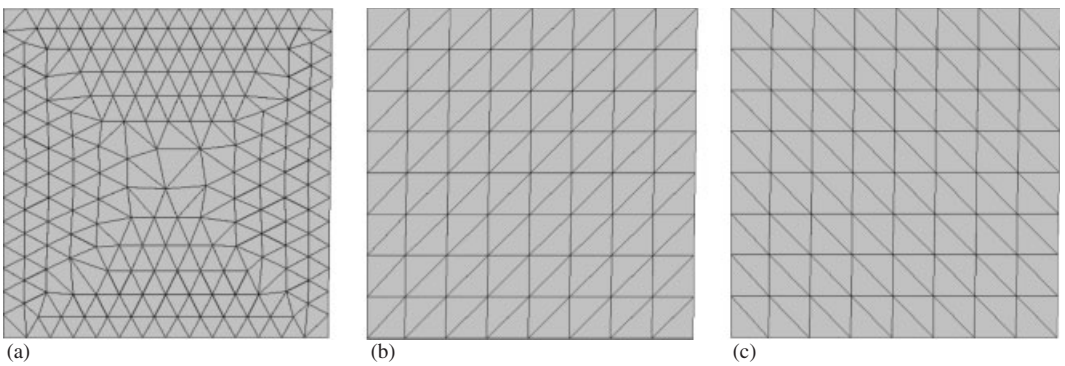

Figure 23. Meshes used in the simulation: (a) 375 elements; (b) 128 elements; and (c) 128 elements.

Three meshes of PGP stabilized triangles ($c = 4$) are considered. The first one, mesh (a), corresponds to a rather arbitrary distribution of 375 elements. The two remaining meshes are structured arrangements of triangles, either following the failure line direction (mesh (b)), or orthogonal to it (mesh (c)). Both of them have 128 finite elements (Figure 23).

The performance of the PGP elements in this test can be evaluated by comparing the equivalent plastic strain field (see Figure 24) and the load–displacement curves (Figure 25(a)) obtained with the meshes (b) and (c). Solution for mesh (a) is not relevant for the load–displacement curve comparison because the size of the finite elements is different from that of meshes (b) and (c). We can observe that both responses (b) and (c) are clearly different. This test shows a similar response to that observed in Section 4.3, though much more marked in this case due to the plastic softening. However, we remark that they represent two extreme conditions. Figure 25(b) demonstrates that even by modifying the stabilization parameter several orders, it is not possible to correct the pathological effect of mesh bias, which confirms that this drawback is due to the deficient kinematical behaviour of the linear triangle.

DOI: 10.1002/cnm

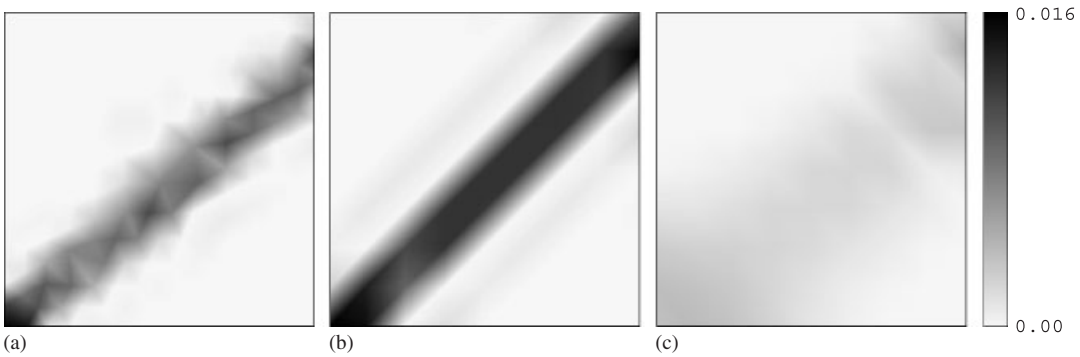

Figure 24. Equivalent plastic strain maps for meshes of Figure 23.

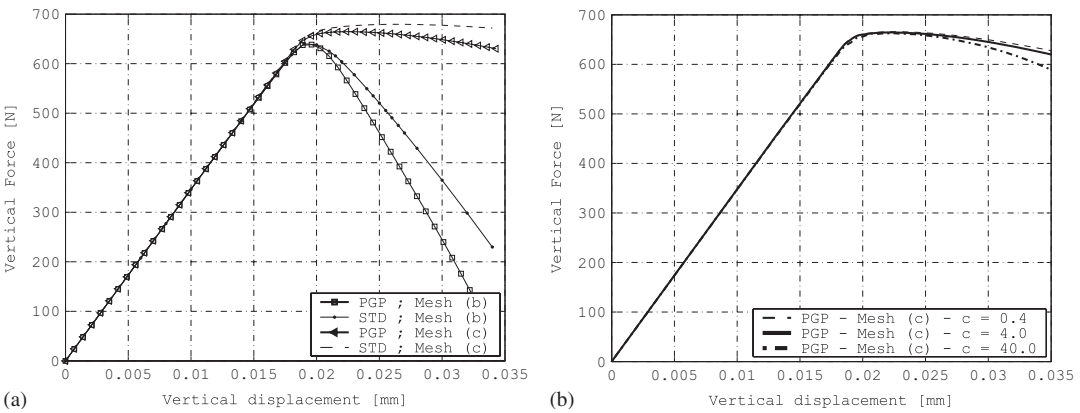

Figure 25. Load–displacement curve.

5. CONCLUSIONS

We have evaluated a stabilized mixed finite element formulation with low-order interpolation which shows good performances for solving small deformation incompressible solid mechanics problems.

If compared with displacement irreducible formulations, the extra computational cost introduced by the additional degree of freedom per node corresponding to the pressure field should be considered. However, the good performance displaying the linear triangles, and mainly the tetrahedral in 3D analysis, makes its use more than acceptable. We remark that the treatment of the vectorial field $\mathbf{\Pi}$, when using the procedure of Equations (28) and (29), does not introduce an appreciable computational cost, because it could be treated as an additional postprocessing step.

Its parallel implementation has also shown a good performance using the sub-domain partitioning method jointly with the Interface–Iterative/Sub domain-Direct technique (IISD) and interface strip (IS) preconditioning. In addition, the use of the IS preconditioner in the context of plastic solids mechanics problems can be considered as an original contribution.

DOI: 10.1002/cnm

From the numerical analysis performed in the strain localization problems, it is necessary to mention an important limitation. Using biased meshes, we have observed some mesh dependence in the plastic localization modelling. We emphasize that this pathological behaviour is insensible to stabilization parameter variations. Although the stabilization scheme incorporates a new sub-scale for displacement field (orthogonal to the standard finite-element scale), this strategy is not enough to enrich the kinematics for capturing, objectively, the characteristic shear band mode with respect to mesh orientation. In contrast with some conclusion reported in the literature, we understand that this is an important aspect of the present formulation which deserves an improvement. Following this idea, the authors have recently proposed the mixed stabilized finite element, here studied, enriched with an elemental supported embedded strong discontinuity kinematics mode, see [26]. This approach opens a feasible future research line for application to ductile material failure.

ACKNOWLEDGEMENTS

This work has received financial support from Consejo Nacional de Investigaciones Científicas y Técnicas (CONICET), Agencia Nacional de Promoción de Actividades Científicas y Tecnológicas (ANPCyT), Universidad Nacional del Litoral (UNL) and Universidad Tecnológica Nacional, all from Argentina, through grants: CONICET PIP 5271; ANPCyT PICT 14573; UNL CAI+D 2005-10-65.

REFERENCES

1. Wall WA, Bischof M, Ramm E. Stabilization techniques for fluid and structural finite elements. *Computational Mechanics*, *New Trends and Applications*. CIMNE: Barcelona, Spain.
2. Klaas O, Maniatty A, Shephard MS. A stabilized mixed finite element method for finite elasticity. Formulation for linear displacement and pressure interpolation. *Computer Methods in Applied Mechanics and Engineering* 1999; **180**:65–79.
3. Chiumenti M, Valverde Q, de Saracibar CA, Cervera M. A stabilized formulation for incompressible elasticity using linear displacement and pressure interpolations. *Computer Methods in Applied Mechanics and Engineering* 2002; **191**:5253–5264.
4. Chiumenti M, Valverde Q, de Saracibar CA, Cervera M. Una formulación estabilizada para plasticidad incompresible usando triangulos y tetraedros con interpolaciones lineales en desplazamientos y presiones. Métodos Numéricos en Ingeniería V.
5. Cervera M, Chiumenti M, Valverde Q, de Saracibar CA. Mixed linear/linear simplicial elements for incompressible elasticity and plasticity. *Computer Methods in Applied Mechanics and Engineering* 2003; **192**:5249–5263.
6. Cervera M, Chiumenti M, de Saracibar CA. Shear band localization via local j_2-continuum damage mechanics. *Computer Methods in Applied Mechanics and Engineering* 2004; **193**:849–880.
7. Valverde Q. Elementos estabilizados de bajo orden en mecánica de sólidos. *Ph.D. Thesis*, UPC, ETSCCP, Barcelona, Spain, 2002.
8. Simo J, Oliver J, Armero F. An analysis of strong discontinuities induced by strain-softening in rate-independent inelastic solids. *Computational Mechanics* 1993; **12**:277–296.
9. Armero F, Garikipati K. An analysis of strong discontinuities in multiplicative finite strain plasticity and their relation with the numerical simulation of strain localization. *International Journal of Solids and Structures* 1996; **33**:2863–2885.
10. Oliver J, Cervera M, Manzoli O. Strong discontinuities and continuum plasticity models: the strong discontinuity approach. *International Journal of Plasticity* 1999; **15**(3):319–351.
11. Regueiro R, Borja R. A finite element model of localized deformation in frictional materials taking a strong discontinuity approach. *Finite Element in Analysis and Design* 1999; **33**:283–315.
12. Codina R. Stabilization of incompressibility and convection through orthogonal sub-scales in finite element method. *Computer Methods in Applied Mechanics and Engineering* 2000; **190**:1579–1599.
13. Storti M, Nigro N, Paz R. PETSc-FEM a general purpose, parallel, multi-physics FEM program. *International Center of Computational Method in Engineering* (CIMEC), http://www.cimec.org.ar/petscfem/

DOI: 10.1002/cnm

14. Storti M, Dalcin L, Paz R, Yommi A, Sonzogni V, Nigro N. A preconditioner for the Schur complement matrix. *Advances in Engineering Software* 2006; **37**(11):754–762.
15. Hughes T. *The Finite Element Method. Linear Static and Dynamic Finite Element Analysis*. Prentice-Hall: Englewood Cliffs, NJ, 1987.
16. Hughes TJR, Franca LP, Balestra M. A new finite element formulation for computational fluid dynamics: V. Circumventing the Babuska–Brezzi condition: a stable Petrov–Galerkin formulation of Stokes problem accommodating equal-order interpolation. *Computer Methods in Applied Mechanics and Engineering* 1985; **59**:85–99.
17. Tezduyar TE, Mittal S, Ray SE, Shih R. Incompressible flow computations with stabilized bilinear and linear equal order interpolation velocity–pressure elements. *Computer Methods in Applied Mechanics and Engineering* 1992; **95**:221–242.
18. Codina R, Blasco J. Stabilized finite element method for the transient Navier–Stokes equations based on a pressure gradient projection. *Computer Methods in Applied Mechanics and Engineering* 2000; **182**:277–300.
19. Balay S, Buschelman K, Gropp WD, Kaushik D, Knepley M, McInnes LC, Smith BF, Zhang H. Petsc home page, http://www.mcs.anl.gov/petsc, 2001.
20. Balay S, Buschelman K, Gropp WD, Kaushik D, Knepley M, McInnes LC, Smith BF, Zhang H. *Petsc Users Manual*, *Technical Report ANL*-95/11—*Revision 2.1.5*, Argonne National Laboratory, 2002.
21. Balay S, Gropp WD, McInnes LC, Smith BF. Efficient management of parallelism in object oriented numerical libraries. In *Modern Software Tools in Scientific Computing*, Arge E, Bruaset AM, Langtangen HP (eds). Birkhauser: Basel.
22. Gropp W, Lusk E, Skeljumm A. Using mpi: portable parallel programming with the message passing interface. *Technical Report*, MIT Press, 1995.
23. Karypis G, Kumar V. Metis 3.0: unstructured graph partitioning and sparse matrix ordering system, 1997.
24. Belytschko T, Bindeman LP. Assumed strain stabilization of the 4-node quadrilateral with 1-point quadrature for nonlinear problems. *Computer Methods in Applied Mechanics and Engineering* 1991; **88**:311–340.
25. Kachanov LM. *Foundation of the Theory of Plasticity*. North-Holland: Netherlands, 1971.
26. Sánchez PJ, Sonzogni VE, Huespe AE, Oliver J. Stabilized mixed finite elements with embedded strong discontinuities for shear band modelling. *Journal of Applied Mechanics* (ASME) 2006; **76**(6):995–1004.

DOI: 10.1002/cnm